Journal of
Synchrotron Radiation

ISSN 0909-0495

Received 21 October 2011
Accepted 6 February 2012

A unique approach to accurately measure thickness in thick multilayers

Bing Shi,[a]* Jon M. Hiller,[b] Yuzi Liu,[c] Chian Liu,[a] Jun Qian,[a] Lisa Gades,[a] Michael J. Wieczorek,[a] Albert T. Marander,[a] Jorg Maser[a,c] and Lahsen Assoufid[a]

[a]X-ray Science Division, Argonne National Laboratory, Argonne, IL 60439, USA, [b]Materials Science Division, Argonne National Laboratory, Argonne, IL 60439, USA, and [c]Center for Nanoscale Materials, Argonne National Laboratory, Argonne, IL 60439, USA. E-mail: shi@anl.gov

X-ray optics called multilayer Laue lenses (MLLs) provide a promising path to focusing hard X-rays with high focusing efficiency at a resolution between 5 nm and 20 nm. MLLs consist of thousands of depth-graded thin layers. The thickness of each layer obeys the linear zone plate law. X-ray beamline tests have been performed on magnetron sputter-deposited WSi_2/Si MLLs at the Advanced Photon Source/Center for Nanoscale Materials 26-ID nanoprobe beamline. However, it is still very challenging to accurately grow each layer at the designed thickness during deposition; errors introduced during thickness measurements of thousands of layers lead to inaccurate MLL structures. Here, a new metrology approach that can accurately measure thickness by introducing regular marks on the cross section of thousands of layers using a focused ion beam is reported. This new measurement method is compared with a previous method. More accurate results are obtained using the new measurement approach.

Keywords: multilayer Laue lenses; focused ion beam; scanning electron microscope; image processing; stitching.

1. Introduction

Multilayer Laue lenses (MLLs) are conceptually capable of focusing X-rays to 1 nm (Kang *et al.*, 2005). In addition, they provide a promising path to focusing hard X-rays with very high focusing efficiency at more moderate resolution between 5 nm and 20 nm. The MLLs developed at Argonne National Laboratory are based on WSi_2/Si multilayers deposited by the DC magnetron sputtering technique (Liu *et al.*, 2007). Other groups have also developed MLLs. WSi_2/Si MLLs have been studied and reported by Wang's group (Zhu *et al.*, 2010); Koyama *et al.* fabricated and characterized MLLs using $MoSi_2$/Si (Koyama *et al.*, 2011); Liese *et al.* reported their work on the fabrication of Ti/ZrO_2 MLLs by a combination of pulsed laser deposition and a focused ion beam (Liese *et al.*, 2010).

MLLs can be fabricated by a variety of methods, and is an area of active research (Liu *et al.*, 2005; Jahedi *et al.*, 2010). To date, a line focus of 16 nm with 31% efficiency (Kang *et al.*, 2008) and a two-dimensional focus spot size of 25 nm × 27 nm (FWHM) with an efficiency of 17% have been achieved with MLLs using 19.5 keV X-rays at the Advanced Photon Source/Center for Nanoscale Materials 26-ID nanoprobe beamline (Yan *et al.*, 2011).

2. New method for layer thickness measurements

MLLs have been successfully studied and characterized. However, key issues remain to develop MLLs that can focus X-rays to below 10 nm. One of these key issues is the lack of an accurate metrology tool for measuring the MLLs' thin layer stack structure. To fabricate an MLL, thousands of depth-graded WSi_2/Si thin layers need to be deposited. These layer thicknesses vary from a few nanometers to several hundred nanometers across the total width of the MLL. The deposited multilayers will be further processed into MLL structures. To protect the deposited multilayers, a sandwich structure is made by pasting another Si wafer on top of the multilayers before dicing and thinning the deposited multilayers into MLLs. M-bond is used as the glue. It is an adhesive that contains two-component epoxy-phenolic resins. The multilayers are then analyzed using a scanning electron microscope (SEM) to characterize the cross section to calibrate the thickness of each layer. More than a dozen images need to be taken to obtain a clear view of the thin layers on these thousands of depth-graded multilayers. The images are processed individually using image processing software and then stitched together. Once the thickness of each layer is measured, the corrective factor of the deposition can be determined. The multilayers with the designed layer thickness can then be deposited.

In the aforementioned image processing method, SEM images were taken one after another such that each image overlapped the previous image. Overlapped areas are required for the stitching of images. They can be clearly distinguished because these areas are darker than the non-overlapping areas owing to electron-beam-enhanced deposition of an organic film. Overlapping cannot be controlled quantitatively. Images were stitched together by estimating the overlapped area of the adjacent images and by looking at the trend lines' slope of $1/d$ (where d is the thickness of two adjacent layers). This is where errors can be introduced. To improve the absolute accuracy of our measurements, we have developed a new

method which involves putting marks on the multilayers to be used as references. The marks work as a ruler on the multilayer structure during the image processing. These marks were created using a focused ion beam (FIB). By applying these marks, the images can be processed much more accurately than before.

A Zeiss 1540XB FIB-SEM was used to make these marks that greatly reduce errors introduced by pattern stitching. Images were taken on samples with and without marks using the SEM attached to the FIB. To obtain high-resolution images for the thin layers, a Hitachi S-4700-II high-resolution field-emission SEM was employed. These acquired images were then processed using image processing software to compare the results.

3. Results and discussion

High-resolution SEM images were taken one after another without marks using the previous method. SEM images of an overview of the multilayers, the thin layers and the thick layers in cross-section view, are shown in Fig. 1. Customized software was used to calculate the thickness of each thin layer after image processing. The resulting calculation on the non-marked multilayers is shown in Fig. 2. The *x*-axis displays the total thickness of the multilayer from the thinner side calculated by adding each layer's thickness. The *y*-axis is $1/d$ (d is the thickness of two adjacent layers). Since $1/d$ *versus* thickness was linear according to the zone plate law when the data were stitched to each other, keeping the linear trend and considering the thickness of the overlapping area were useful tools. Because the stitching process is determined by estimation, different results can be achieved from the same images. Each differently colored data group was obtained from each image processing step.

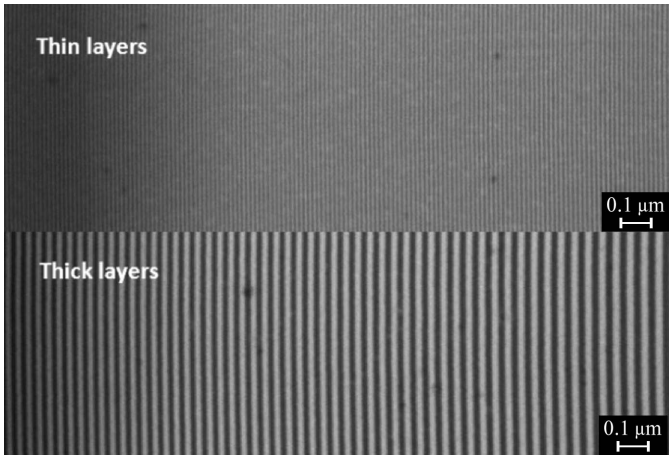

Figure 1
SEM images of the cross section of WSi_2/Si multilayers. White layers are WSi_2; black layers are Si.

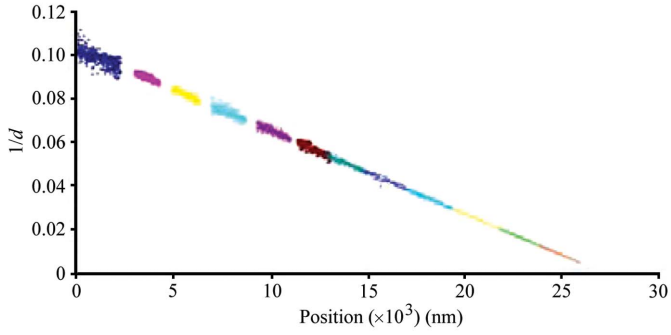

Figure 2
Thickness calculation results from SEM image processing.

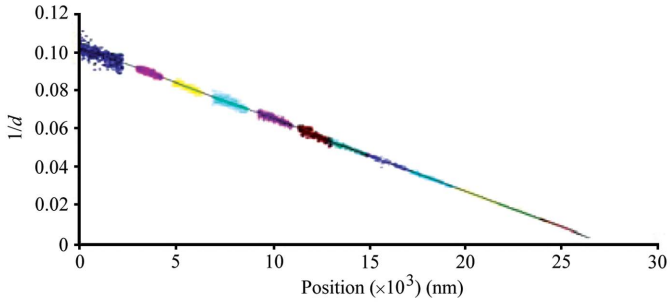

Figure 3
Thickness calculation results from SEM image processing with trend lines.

There were gaps between the images of the thin layers. These gaps were due to the low contrast caused by the electron-beam-enhanced deposition of an organic film created during the SEM analysis; the M-bond in the MLL sandwich structure led to the organic contamination. We believe that the interaction of the primary beam with the hydrocarbons from the M-bond in the SEM chamber resulted in the deposition of a hydrocarbon film. Longer exposure time to the beam produced thicker hydrocarbon contamination layers and darker images. Overlapping between the images increases the darkness and some of the overlapped areas were too dark to be processed. Because the overlapped distances could not be measured, they were estimated by adding trend lines to the image processing results and stitching the images together as 'reasonably' as possible. This also introduced errors owing to the assumption that the multilayer structure obeyed the linear zone plate law (Fig. 3).

The new method used a FIB to mark the multilayer samples. An overview SEM image of an FIB-marked sample is shown in Fig. 4. Line marks were obtained by ion-milling using gallium ions. An 'X' was created near the lines to make identification easier under an optical microscope. The lines are spaced exactly 2 µm apart from each other. The distance and the shape of the marks can be changed as needed (Fig. 4). By making these marks, stitching can be performed more accurately. Separate SEM images were taken with two marks in each image (Fig. 5). The distance between lines can be changed as required and the lines can be made narrower (Figs. 6 and 7).

Even if one or more of the images are not useful for calculations, selective images can be obtained instead of taking a whole set of images as required by the previous processing method. The image processing data are shown in Fig. 8.

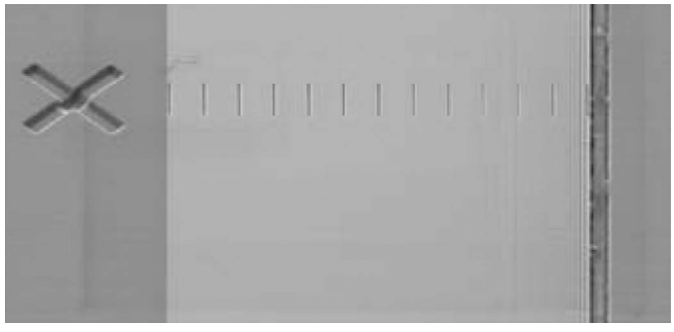

Figure 4
SEM images of the samples with FIB line marks made every 2 µm.

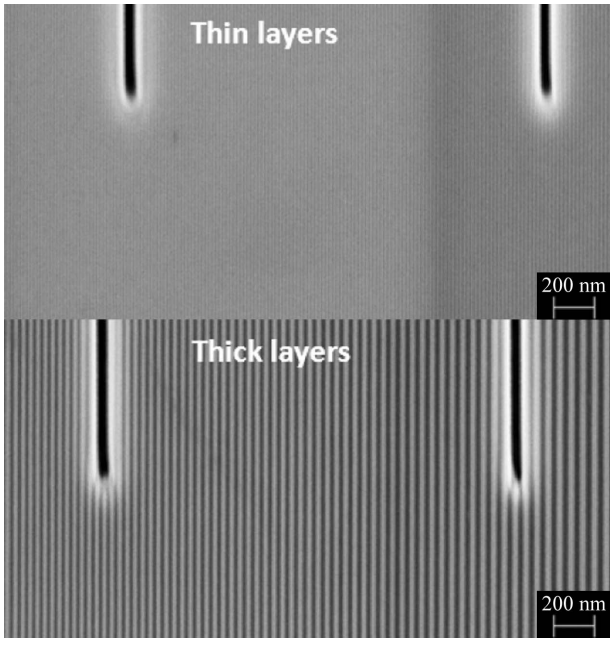

Figure 5
SEM images with marks.

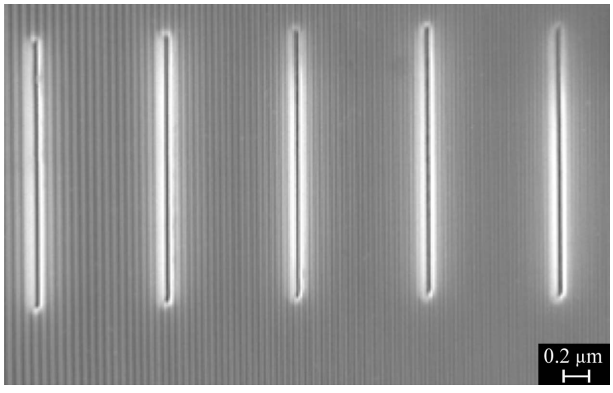

Figure 6
Line distance changed to 1 μm.

4. Conclusions

We report a new metrology method using a FIB to make marks on the cross sections of MLL samples which possess grading thicknesses from a few nanometers to hundreds of nanometers. The total thickness of a multilayer is over 20 μm. The FIB marking method is a simple approach used to improve characterization of the MLLs structure. With marks, SEM image processing can achieve accurate results for stitching films.

The SEM analysis work was performed at the Electron Microscopy Center of Argonne National Laboratory. This work is supported by the US Department of Energy, Office of Science, under Contract No. DE-AC02-06CH11357.

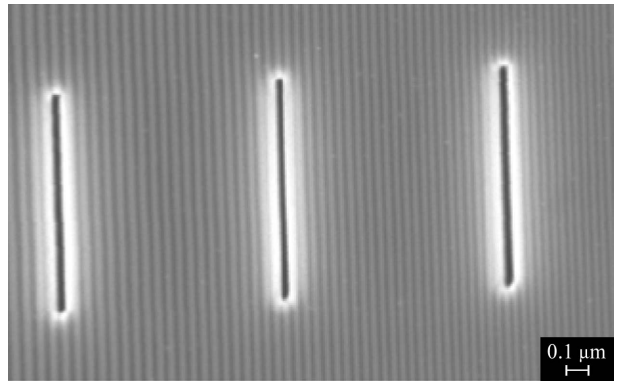

Figure 7
1 μm line distance with shorter lines.

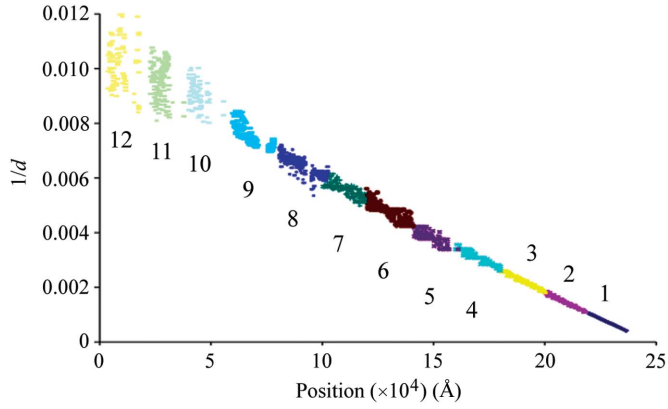

Figure 8
Thickness calculation results from SEM image processing with the marks. The numbers 1–12 refer to the image number.

References

Jahedi, N., Conley, R., Shi, B., Qian, J., Lauer, K. & Macrander, A. T. (2010). *Nucl. Instrum. Methods Phys. Res. A*, **616**, 89–92.
Kang, H. C., Stephenson, G. B., Liu, C., Conley, R., Macrander, A. T., Maser, J., Bajt, S. & Chapman, H. N. (2005). *Appl. Phys. Lett.* **86**, 151109.
Kang, H. C., Yan, H., Winarski, R. P., Holt, M., Liu, C., Conley, R., Vogt, S., Macrander, A. T. & Stephenson, G. B. (2008). *Appl. Phys. Lett.* **92**, 221114.
Koyama, T., Takenaka, H., Ichimaru, S., Ohchi, T. & Tsuji, T. (2011). *AIP Conf. Proc.* **1365**, 24–27.
Liese, T., Radisch, V. & Krebs, H. U. (2010). *Rev. Sci. Instrum.* **81**, 073710.
Liu, C., Conley, R., Macrander, A. T., Maser, J., Kang, H. C., Zurbuchen, M. A. & Stephenson, G. B. (2005). *J. Appl. Phys.* **98**, 113519.
Liu, C., Conley, R., Qian, J., Kewish, C. M., Macrander, A. T., Maser, J., Kang, H. C., Yan, H. & Stephenson, G. B. (2007). *Nucl. Instrum. Methods Phys. Res. A*, **582**, 123–125.
Yan, H., Rose, V., Shu, D., Lima, E., Kang, H. C., Conley, R., Liu, C., Jahedi, N., Macrander, A. T., Stephenson, G. B., Holt, M., Chu, Y. S., Lu, M. & Maser, J. (2011). *Opt. Express*, **19**, 15069–15076.
Zhu, J., Huang, Q., Li, H., Xu, J., Wang, X., Zhang, Z., Wang, Z. & Chen, L. (2010). *Chin. Opt. Lett.* **8**, 174–176.